

# False Alarm Rate based Statistical Detection Limit for Astronomical Photon Detectors

Albert Wai Kit Lau<sup>1,3,\*</sup>, Leo W.H. Fung<sup>2,3</sup>, and George F. Smoot<sup>4,5,6,7,8,9,10</sup>

<sup>1</sup>*Dunlap Institute for Astronomy and Astrophysics, University of Toronto, Toronto, Canada*

<sup>2</sup>*Institute for Computational Cosmology & Centre for Extragalactic Astronomy, Durham University, Stockton Rd, Durham DH1 3LE, UK*

<sup>3</sup>*Institute for Advanced Study, The Hong Kong University of Science and Technology, Clear Water Bay, Kowloon, Hong Kong*

<sup>4</sup>*Institute for Advanced Study, The Hong Kong University of Science and Technology, Clear Water Bay, Kowloon, Hong Kong, emeritus*

<sup>5</sup>*Energetic Cosmos Laboratory, Nazarbayev University, Astana, Kazakhstan, emeritus*

<sup>6</sup>*Department of Physics, University of California, Berkeley, California, USA, emeritus*

<sup>7</sup>*Laboratoire APC-PCCP, Université Sorbonne Paris Cité, Université Paris Diderot, emeritus*

<sup>8</sup>*Department of Physics, University of California, Berkeley, California, USA, emeritus*

<sup>9</sup>*Laboratoire Astroparticule et Cosmologie, Université de Paris, F-75013, Paris, France, emeritus*

<sup>10</sup>*Donostia International Physics Center, University of the Basque Country UPV/EHU, E-48080 San Sebastian, Spain*

\*Corresponding author: [awk.lau@utoronto.ca](mailto:awk.lau@utoronto.ca)

September 25, 2024

## Abstract

In ultra-fast astronomical observations featuring fast transients on sub- $\mu\text{s}$  time scales, the conventional Signal-to-Noise Ratio (SNR) threshold, often fixed at  $5\sigma$ , becomes inadequate as observational window timescales shorten, leading to unsustainably high False Alarm Rates (FAR). We provide a basic statistical framework that captures the essential noise generation processes relevant to the analysis of time series data from photon-counting detectors. In particular, we establish a protocol of defining detection limits in astronomical photon-counting experiments, such that a FAR-based criterion is preferred over the traditional SNR-based threshold scheme.

We develop statistical models that account for noise sources such as dark counts, sky background, and crosstalk, and establish a probabilistic detection criterion applicable to high-speed detectors. We compare the performance of several detector technologies, including photon-counting CMOS/CCDs, SPADs, SiPMs, and PMTs, in detecting faint astronomical signals. These findings offer insights into optimizing detector choice for future ultra-fast astronomical instruments and suggest pathways for improving detection fidelity under rapid observational conditions.

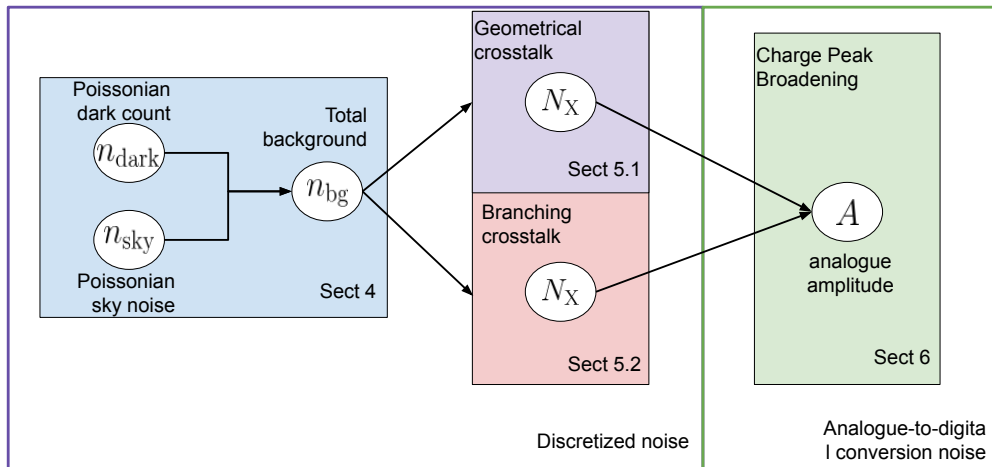


Figure 1: A flowchart of the noise model presented in this work. Starting from a model of the total background noise, we gradually introduce 2 models of detector crosstalk. Building on top of this discretized noise-trigger counting model, we finally proceed to provide a more realistic, continuous model that describe the electronic signal received in the detector.

## 1 Introduction

Table 1: A dictionary of all the mathematics notations.

Notation	Meaning	Units
$n_{\text{dark}}$	Dark count noise rate	Counts per second
$n_{\text{sky}}$	Sky background count rate	Counts per second
$n_{\text{bg}}$	Total background count rate	Counts per second
$\delta t$	Detector integration time	Seconds
$p_{\text{cross}}$	Detector crosstalk probability	$\setminus^a$
FAR	False Alarm Rate	Alarms per second
$N_{\text{det}}$	Detector output count	Counts
$N_{\text{thr}}$	Alarming threshold count	Counts
$N_X$	Crosstalk-affected count	Counts
$A_{\text{det}}$	Detector output analogue signal amplitude	ADU <sup>b</sup>
$A_{\text{thr}}$	Alarming threshold analogue signal amplitude	ADU <sup>b</sup>
$\gamma_{\text{thr,det}}$	Alarming threshold in detected photons	photons
$\gamma_{\text{thr,in}}$	Alarming threshold in photons input on detector	photons
$R_n$	Read noise of detector system	$e^-$ equivalent
$g$	conversion gain of detector system	ADU <sup>b</sup> per photon detected
$k$	Noise correlation factor of detector	$\setminus^a$ , [0,1] typical
QE	Quantum efficiency of detector	%
$\langle \cdot \rangle$	Expectation of random variable $\cdot$	Same as the random variable $\cdot$
$\text{Pr}(\cdot)$	Probability mass/density of random variable $\cdot$	$\setminus^a$

<sup>a</sup>Unit-less or undefined unit

<sup>b</sup>Arbitrary Detector Output Unit

In astronomical observations, the detection criterion is typically defined by a Signal-to-Noise Ratio (SNR) greater than 5, often referred to as the  $5\sigma$  criterion. Assuming normally distributed noise, this threshold corresponds to a confidence level of 99.9999713% - equivalently 3 parts in 10 millions, which is generally reliable in most observational contexts. However, as we shorten the observational window timescale, especially in the realm of ultra-fast astronomy, this approach becomes less practical due to the increase of false alarms.

Ultra-fast astronomical observations focus on timescales ranging from milliseconds to nanoseconds [15]. For example, continuous observations at a timescale of 1 *ms* over an entire night (approximately 50,000 seconds) result in capturing  $5 \times 10^7$  frames. Using the  $5\sigma$  criterion, which corresponds to a false alarm probability of less than 0.0000287%, would yield around 1,000 false alarms per night, identically almost one per minute. As the observational timescale decreases to 1 *ns*, the number of frames captured increases to  $5 \times 10^{13}$ , resulting in an overwhelming  $10^9$  false alarms per night, or approximately 20,000 false alarms per second.

This high false alarm rate is clearly unsustainable. The rate of false alarms is directly tied to the observational timescale, making the use of a fixed SNR criterion inadequate for ultra-fast observations. Instead, a more practical approach is to adopt a fixed false alarm rate (FAR). In ultra-fast astronomy, a typical criterion might allow one false alarm per  $10^7$  seconds, while other applications may employ thresholds of one false alarm per  $10^5$  seconds, per night ( $\sim 5 \times 10^4$  seconds), or even per hundred nights ( $\sim 5 \times 10^6$  seconds). In the subsequent sections, we will explore the effectiveness and application of these FAR-based criteria in the context of ultra-fast astronomical detection.

## 2 Photon Counting Detectors and Single-Photon Detectors

Before diving into the statistics, we would first review detectors used in astronomical observation. Conventional optical detectors, such as photographic films and most CCDs, are unable to produce a discernible signal upon detecting a single photon due to high input-referred noise. This noise is typically larger than the signal generated by a single photon (commonly referred to as an  $e^-$ , as most detectors convert photon absorption into electron excitation). When a sufficient number of photons are detected, the output signal can be approximated by a normal distribution, provided that enough photons are collected.

With advancements in detector technology, modern sensors such as EMCCDs, CCDs, and sCMOS are achieving intrinsic gains or reduced readout noise levels that bring input-referred noise well below 1  $e^-$  [5, 22, 2, 10]. At these low noise levels, the output signal deviates from the normal distribution, revealing the quantized nature of photons [21].

Beyond photon counting, certain detectors are capable of single-photon detection, where individual photons are measured as they arrive. This capability allows for the determination of additional properties, such as photon arrival time and correlations between multiple photons. Single-photon detectors must operate with response and readout times on the order of microseconds or nanoseconds. Technologies such as photomultiplier tubes (PMTs) [8], silicon photomultipliers (SiPMs) [3], transition-edge sensors (TES) [9], and microwave kinetic inductance detectors (MKIDs) [16, 20] are examples of such systems. Certain detec-

tors, like MKIDs, can even discern the energy (or wavelength) of individual photons [16]. These technologies are evolving into array configurations with imaging capabilities, making them increasingly essential for a wide range of applications in astronomical research. These detectors may have different types of noise compared to Conventional optical detectors, which we will introduce and formulate in the subsequent sections.

### 3 False Alarm Rate based Detection Limit for high speed sensors

We are interested in the astrophysical use case, in which there is a sudden increment in detected photon. This sudden increment in detected photon can both be driven by stochastic noise fluctuation or physical astronomical phenomena. Of scientific interest, we would like to separate between the two scenarios. In particular, we would like to set an integrated photon count threshold  $N_{\text{thr}}$  (over some integration time window  $\delta t$ ), so that exceeding the threshold ( $> N_{\text{thr}}$ ) would result in a trigger/alarm for follow-up analysis. The detection limit in this trigger/alarm based setting can be established by imposing a False Alarm Rate (FAR) limit, which restricts the frequency of noise-triggered alarms.

To establish a statistical formulation of the FAR criterion, we first define a threshold for the received photon counts  $N_{\text{thr}}$ . Consider a single-pixel sensor with characteristic parameters (such as dark count rate, sensitivity and so on, which we will elaborate in the following sections), observing a patch of sky with an averaged background photon rate  $\langle n_{\text{bg}} \rangle$  over a time bin of  $\delta t$ , and searching for a photon burst. The expected false alarm probability per time bin is given by:

$$Pr(N_{\text{det}} \geq N_{\text{thr}} | \delta t, \langle n_{\text{sky}} \rangle, \langle n_{\text{dark}} \rangle, p_{\text{cross}}) \leq \text{FAR} \cdot \delta t \quad (1)$$

The above equations are formulated for detecting photon excess; we can similarly derive the statistical equations for detecting photon deficit, as discussed in Appendix A.

It is also important to note that the above equations calculate the FAR for a single resolution element of the sky. When the detector has imaging capabilities, the probability must be multiplied by a factor of  $\frac{\text{sensor area}}{\text{resolution element size}}$ . This implies that the detection threshold increases as the FAR is distributed across the entire sensor area.

### 4 Dark-Count Noises and Sky Backgrounds

Realistic detectors always exhibit some level of thermal noise. In traditional detectors like CCDs, electrons excited by thermal fluctuations are captured, resulting in dark current, commonly measured in units of  $e^-/s$ . In single-photon detectors, electrons excited by thermal fluctuations on the detection surface are amplified in the same way as those excited by incident photons, producing output pulses that are indistinguishable from genuine photon events. These false detections are referred to as dark counts and are a primary source of noise in single-photon detectors.

The probability of registering  $N_{\text{dark}}$  dark counts (or  $N_{\text{dark}} e^-$  dark current) within a time interval  $\delta t$  can be modeled by a Poisson distribution [7]:

$$\Pr(N_{\text{dark}}|\langle n_{\text{dark}}\rangle, \delta t) = \frac{(\langle n_{\text{dark}}\rangle \delta t)^{N_{\text{dark}}} \exp(-\langle n_{\text{dark}}\rangle \delta t)}{N_{\text{dark}}!} \quad (2)$$

It is important to note that variations in the fabrication process can lead to different regions or pixels of the detector exhibiting different dark count rates, resulting in non-uniform noise characteristics across the detector.

The noise contribution from the sky background, as well as from other background sources, can be modeled similarly to dark counts using the Poisson distribution. However, factors such as the optical system’s efficiency, the collection area, and the detector’s sensitivity must also be considered. For such case we can simply replace  $\langle n_{\text{dark}}\rangle$  with  $\langle n_{\text{bg}}\rangle = \langle n_{\text{dark}}\rangle + \langle n_{\text{sky}}\rangle$  into the above equation.

## 5 Crosstalk and Afterpulse

In some single-photon detectors, a single photon can be mistakenly detected as multiple photons arriving simultaneously, producing an output amplitude several times greater than the expected pulse amplitude from a single photon event. This type of false detection is referred to as crosstalk noise, which originates from residual charge or re-emission during avalanche amplification. Since crosstalk can only occur following the detection of a photon signal or noise event, it is classified as secondary noise [6].

Various models exist to describe the probability of crosstalk, though not all provide straightforward analytical solutions. In this context, we introduce two commonly used models: the Geometric crosstalk model and the Branching crosstalk model [6, 23].

### 5.1 Geometric Crosstalk Model

In the Geometric crosstalk model, a single signal or noise detection event can trigger crosstalk only once. However, the noise generated by crosstalk may in turn trigger additional crosstalk events, making the total number of detected “photon counts” follow a geometric distribution. When there are  $N$  photon signal or noise events, the probability of detecting a total of  $M$  counts is given by:

$$\Pr(N_{\text{X}}|N_{\text{bg}}) = \binom{N_{\text{X}} - 1}{N_{\text{bg}} - 1} (1 - p_{\text{cross}})^{N_{\text{bg}}} (p_{\text{cross}})^{N_{\text{X}} - N_{\text{bg}}}. \quad (3)$$

Here,  $p_{\text{cross}}$  represents the crosstalk probability.

And therefore, given a total background rate  $\langle n_{\text{bg}}\rangle$  and a fixed integration time  $\delta t$ , we can derive the distribution of the marginalized, crosstalk-affected count:

$$\Pr(N_{\text{X}}|\langle n_{\text{bg}}\rangle, \delta t) = \sum_{N_{\text{bg}}=1}^{N_{\text{X}}} \Pr(N_{\text{X}}|N_{\text{bg}}) \Pr(N_{\text{bg}}|\langle n_{\text{bg}}\rangle, \delta t) \quad (4)$$

## 5.2 Branching Crosstalk Model

In the Branching crosstalk model, a single signal or noise detection event may trigger crosstalk multiple times, and the noise generated from crosstalk can, in turn, trigger further crosstalk events. The crosstalk probability in this model can be described using the Borel–Tanner distribution:

$$\Pr(N_X|N_{bg}) = \frac{N_{bg} (\lambda N_X)^{N_X - N_{bg}} \exp(-\lambda N_X)}{N_X (N_X - N_{bg})!} \quad (5)$$

Where  $\lambda = -\log(1 - p_{cross})$ .

Similar to the Geometric model, we can combine the Branching crosstalk model with the event distribution. Assuming the event distribution follows a Poisson process (e.g., primarily driven by dark and background counts), the combined probability forms a generalized Poisson distribution [23]:

$$\begin{aligned} & \Pr(N_X|\langle n_{bg} \rangle, \delta t) \\ & \sum_{N_{bg}=1}^{N_X} \Pr(N_X|N_{bg})\Pr(N_{bg}|\langle n_{bg} \rangle, \delta t) \\ & = \frac{\langle n_{bg} \rangle \delta t (\langle n_{bg} \rangle \delta t + \lambda N_X)^{N_X+1} \exp(-\langle n_{bg} \rangle \delta t - \lambda N_X)}{N_X!} \end{aligned} \quad (6)$$

Other types of secondary noise in photon detectors, such as afterpulses and delayed crosstalk, behave similarly to crosstalk. These phenomena are often caused by optical reflections or trapped charge carriers during avalanche detection [18]. Both afterpulses and delayed crosstalk generate a secondary output pulse shortly after the primary one. Since the delay time of the secondary pulse is generally much shorter than the binning time  $\delta t$ , they can be modeled using the same crosstalk frameworks, where  $p_{cross}$  now represents the combined probability of all secondary noise sources, including crosstalk, afterpulses, and delayed crosstalk.

In practice, crosstalk probabilities usually fall between the Geometric and Branching models, with the actual distribution depending on the detector design. Most well-designed single-photon detectors exhibit secondary noise characteristics that closely follow the Geometric crosstalk model [11]. Therefore, we will use the Geometric crosstalk model, as described in Eq. 4, for further calculations in this manuscript.

## 6 Analogue-to-Digital Conversion and Amplification Noise

Photon detectors convert incoming photons into an electronic signal, such as charge or voltage, and the readout system converts these into digital numbers or pulses. For realistic detectors' output, we rewrite the FAR equation in terms of signal amplitude  $A_{det}$  recorded by the readout system:

$$\Pr(A_{det} \geq A_{thr} | \delta t, n_{sky}, n_{dark}, p_{cross}) \leq \text{FAR} \cdot \delta t \quad (7)$$

The challenge lies in expressing  $Pr(A_{\text{det}})$  in terms of  $Pr(N_{\text{det}})$ , which we can obtain from the discrete noise model above; using the total probability theorem:

$$\Pr(A_{\text{det}}) = \sum_{N_{\text{det}}} \Pr(A_{\text{det}}|N_{\text{det}})\Pr(N_{\text{det}}) \quad (8)$$

Here,  $\Pr(A_{\text{det}}|N_{\text{det}})$  represents the output amplitude distribution given a known photon count detected  $N_{\text{det}}$ , determined by the sensor's characteristics.

In ideal photon-counting or single-photon detectors, the output amplitude is expected to be an integer multiple of the gain, as photon count is quantized and the gain is typically fixed. Therefore, when plotting the output amplitude as a histogram, discrete lines, known as photoelectron (P.E.) peaks, should appear. A 1 P.E. peak corresponds to the output amplitude from a single detected photon, a 2 P.E. peak corresponds to the output from two detected photons, and so forth.

In practice, several factors can prevent the output of a photon detector from being perfectly quantized. These factors include gain variations across different pixels or regions of the detector, photon arrivals during pixel recovery time (particularly in avalanche-based single-photon detectors), and readout noise from the electronics. As a result, the charge spectrum of the output pulse is broadened in realistic photon detectors.

Rather than modeling each factor individually, we can combine these effects into an overall broad statistical distribution. Typically, we use Gaussian distributions for this purpose, as most random factors and electronic noise tend to exhibit Gaussian-like behavior. Thus, the histogram of the output broadens from discrete lines into a mixture of Gaussian distributions, which is commonly referred to as the Gaussian Mixture Model (GMM) [17, 1]. Using this model, we can express the desired output amplitude distribution given a known photon count detection,  $Pr(A_{\text{det}}|N_{\text{det}})$ .

A normalized Gaussian distribution requires two parameters: the mean ( $\mu$ ) and the standard deviation ( $\sigma$ ). For  $N$  different P.E. peaks,  $2N$  parameters are required to model the broadening effect. However, we can reduce the number of dependent parameters for GMM fitting by leveraging the inherent properties of the detectors: (1) the linear conversion gain,  $g = \mu_1$ , and (2) the standard deviation of each Gaussian peak,  $\sigma_n$ , which grows with the peak number according to an exponential factor  $k$  for noise correlation. Typically,  $k$  lies between 0 and 1 [4]. Mathematically, we can express this as  $\mu_n = g \cdot n$  and  $\sigma_n = \sigma_1 \cdot n^k = R_n \cdot g \cdot n^k$  (here we use  $R_n \cdot g$  to represent  $\sigma_1$  for agreement to common convention in CCD/CMOS noise, which we will show). This allows us to reduce the model to just three key parameters:  $g$ ,  $R_n$ , and  $k$ , which can vary with the detector model and must be determined experimentally. For semiconductor avalanche-based detectors,  $k$  is typically around 0.5 [11], representing the Gaussian randomness inherent in the avalanche process, while vacuum tube detectors like PMT may have  $k$  approaching 1, indicating a worse photon resolving power.

Thus, the statistical expression for the GMM model is:

$$\Pr(A_{\text{det}}|N_{\text{det}}) = \frac{1}{\sqrt{2\pi \cdot R_n \cdot g \cdot N_{\text{det}}^k}} e^{-\frac{(A_{\text{det}} - g \cdot N_{\text{det}})^2}{2(R_n \cdot g \cdot N_{\text{det}}^k)^2}} \quad (9)$$

In common CCD and CMOS detectors, noise originating from the readout electronics, commonly referred to as read noise ( $R_n$ ), arises from the electronics responsible for powering

and reading data from the detector. This type of noise is typically independent of integration time. Read noise can also be modeled using the Gaussian Mixture Model (GMM) described above.

Unlike avalanche-based detectors, where randomness in the avalanche process leads to variable noise, CCD and CMOS detectors exhibit a more consistent behavior since there is no avalanche-related randomness. As a result, the read noise remains constant, regardless of the number of photons collected (i.e., the peak number). Therefore, we can simplify the model by setting the exponential growth factor  $k = 0$ , which implies that the standard deviation remains constant across all peaks. Traditionally, this read noise  $R_n$  of CCD/CMOS is reported in the unit of  $e^-$  equivalent, i.e. electrons excited by photon detected. Following this convention, we express the GMM variance as  $\sigma_1 = \sigma_2 = \dots = \sigma_N = R_n \cdot g$ , together with the conversion gain  $g$  of the detector.

## 7 Detection Limit Simulation

To quantify the detection limits of high-speed astronomical detectors, we integrate the statistical models developed in the previous sections into a numerical simulation. The goal is to evaluate the performance of various detectors under different observational conditions, particularly focusing on their ability to detect faint astronomical signals over ultra-fast timescales.

Here, we wish to calculate the distributional properties of the detector signal amplitude  $A_{\text{det}}$  given a pre-determined background noise rate  $\langle n_{\text{bg}} \rangle$  and a window size  $\delta t$ . This distribution would provide insight in quantifying the amount of false event triggers driven solely by various noise. Using the equations derived earlier, we compute the detection threshold for each detector by propagating the signal amplitude distribution, incorporating both intrinsic detector noise and external noise sources. To capture the combined effects of dark counts, background noise, and crosstalk across different detector types, we employ the formulations for  $\Pr(N_{\text{dark}}|\langle n_{\text{dark}} \rangle, \delta t)$ ,  $\Pr(N_{\text{X}}|N_{\text{bg}})$  and  $\Pr(A_{\text{det}}|N_{\text{det}})$  from Eq. 2, 4, and 9, respectively. These terms are then propagated to obtain the overall probability density of the detector's output amplitude by combining Eq. 4 and 8:

$$\Pr(A_{\text{det}}|\langle n_{\text{bg}} \rangle, \delta t) = \sum_{N_{\text{det}}}^{\infty} \sum_{N_{\text{bg}}=1}^{N_{\text{det}}} \Pr(A_{\text{det}}|N_{\text{det}}) \Pr(N_{\text{det}}|N_{\text{bg}}) \Pr(N_{\text{bg}}|\langle n_{\text{bg}} \rangle, \delta t) \quad (10)$$

Finally, we compare this probability density of the detector's output amplitude with the desired false alarm rate, as defined by Eq. 7, to determine the detection threshold  $A_{\text{thr}}$ .

Before evaluating the distribution of  $A_{\text{det}}$ , we would like to introduce a few quantities that are re-scaled from  $A_{\text{det}}$ , with the purpose of comparing the performance between different detector technologies on equal footing. The detection threshold  $A_{\text{thr}}$  can be expressed in terms of the detector's conversion gain  $g$ , which allows us to compute the corresponding photon count threshold for detected signals:

$$\gamma_{\text{thr,det}} = \left[ \frac{A_{\text{thr}}}{g} \right] \quad (11)$$

Here,  $\gamma_{\text{thr, det}}$  represents the minimum number of photons that must be detected to surpass the noise floor. To facilitate a comparison between different detector technologies, we further normalize the detection threshold by the detector’s quantum efficiency (QE), yielding:

$$\gamma_{\text{thr,in}} = \left\lceil \frac{A_{\text{thr}}}{g \cdot (\text{QE})} \right\rceil \quad (12)$$

This normalization accounts for variations in the quantum efficiencies and conversion gains across detectors, enabling a fair comparison of their intrinsic performance.

We implemented the simulation using a Python-based framework to model and compare several commonly used detectors in astronomical observations. The key detector types evaluated in the simulation are:

- Photon-counting CMOS/CCD detectors [10]
- Single-Photon Avalanche Diodes (SPAD) [19]
- Silicon Photomultipliers (SiPM) [12, 13]
- Photomultiplier Tubes (PMT) [14]

For the simulation, we assume a typical sky background rate of  $\langle n_{\text{sky}} \rangle = 100$  photons per second onto the detector. The typical detector parameters are shown in Table 2.

Table 2: Detector Parameters for Simulation

Detector parameters	photon counting CMOS/CCD	SPAD	SiPM	PMT
$n_{\text{dark}}$ (Counts per second)	0.01	100	1000	100
$p_{\text{cross}}$	0	0.01	0.1	0.03
$g$ ( $ADU^c$ per photon detected)	10	$10^4$	$10^6$	$10^5$
$R_n$ ( $e^-$ Eqv.)	0.3	0	0.1	0.1
k	0	0	0.5	1
Q.E. (%)	85	50	35	20

<sup>c</sup>Here the ADU chosen is in fact  $e^-$  after amplification

We also assume that there is no lower limit on the frame time for the detectors, though this is not realistic in practical applications. Photon detectors like SiPM or PMT can operate on nanosecond timescales, while CMOS/CCD detectors typically have a frame rate limit of around 1,000 frames per second (fps).

Using the detector specifications in Table. 2, we determine the detection threshold by considering a fixed FAR budget of  $\text{FAR} = \text{one false alarm per } 10^7 \text{seconds}$ , and express the threshold for each detectors in terms of  $\gamma_{\text{thr,in}}$ . Fig. 2 illustrates the detection limits of these detectors in terms of photon counts arriving at the detector surface (equivalently  $\gamma_{\text{thr,in}}$ ). From this figure, it is evident that CMOS/CCD detectors offer superior sensitivity due to their higher quantum efficiency, lower dark noise, and absence of crosstalk. However, their slower frame rates and inter-frame dead times make them unsuitable for ultra-fast observations.

SPAD detectors also seems to demonstrate good performance in the ultra-fast regime, but they suffer from dead times on the microsecond scale, limiting their ability to detect

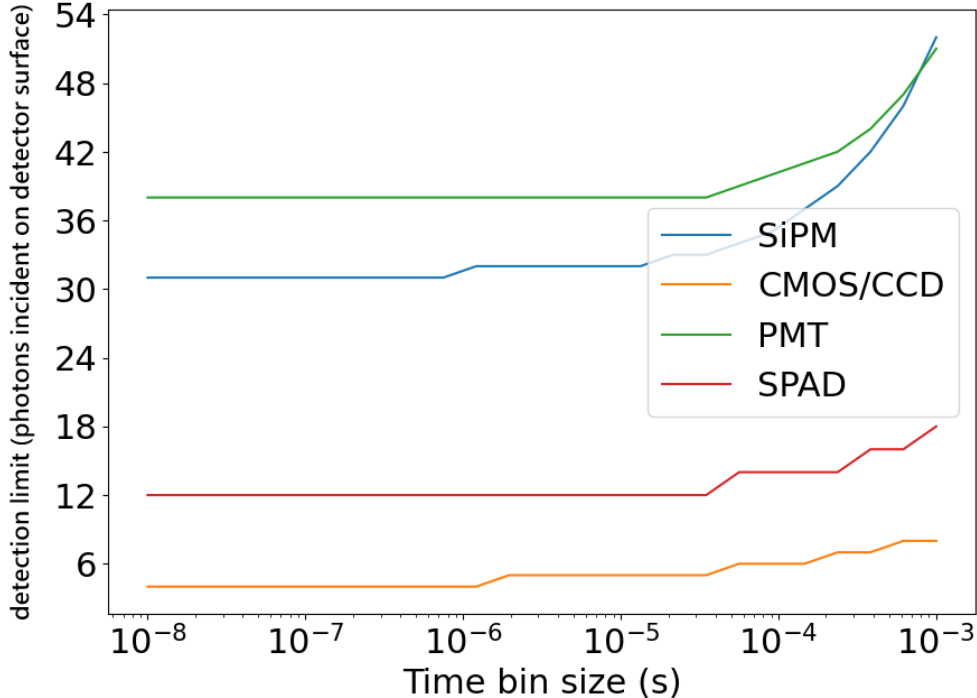


Figure 2: Detection limit of detectors in photon counts arriving at the detector surface  $\gamma_{\text{thr,in}}$ , as a function of the time bin/window size  $\delta t$ . Note however that the performance of photon counting CMOS/CCD should be downgraded to account for the slow frame rate and inter-frame dead time, effectively making the continuous ultra-fast monitoring unsustainable on those devices.

multiple photons arriving simultaneously. Meanwhile, SiPM and PMT detectors exhibit higher detection limits but can resolve multiple photons within a few nanoseconds. Among these, SiPM detectors perform slightly better at shorter timescales because their photon-resolving capability (exponential factor  $k$ ) does not degrade as rapidly with concurrent photon arrivals compared to PMTs.

## 8 Conclusion

This work introduces a statistically driven methodology for determining detection limits in photon detectors used in ultra-fast astronomical observations. By shifting from a traditional Signal-to-Noise Ratio (SNR) threshold to a False Alarm Rate (FAR)-based detection criterion, we address the challenge of managing false positives that arise from reducing observational timescales. The FAR-based model, grounded in Poisson statistics and generalized to account for dark counts, sky background, and crosstalk noise, provides a more reliable approach for high-speed astronomical detection. Our statistical framework was applied to different detector technologies, and simulations revealed significant differences in performance. This approach can be generalized to evaluate future detector technologies and observational strategies, ensuring that false alarm rates are controlled while maintaining the sensitivity

required for detecting transient astronomical events.

### Acknowledgements

The Dunlap Institute is funded through an endowment established by the David Dunlap family and the University of Toronto.

## References

- [1] V. Álvarez, M. Ball, F. Borges, S. Cárcel, J. Castel, S. Cebrian, A. Cervera, C. Conde, T. Dafni, T. Dias, et al. Design and characterization of the SiPM tracking system of NEXT-DEMO, a demonstrator prototype of the NEXT-100 experiment. *Journal of Instrumentation*, 8(05):T05002, 2013.
- [2] A. Boukhayma, A. Peizerat, and C. Enz. Noise reduction techniques and scaling effects towards photon counting CMOS image sensors. *Sensors*, 16(4):514, 2016.
- [3] P. Buzhan, B. Dolgoshein, L. Filatov, A. Ilyin, V. Kantzerov, V. Kaplin, A. Karakash, F. Kayumov, S. Klemin, E. Popova, et al. Silicon photomultiplier and its possible applications. *Nuclear Instruments and Methods in Physics Research Section A: Accelerators, Spectrometers, Detectors and Associated Equipment*, 504(1-3):48–52, 2003.
- [4] G. Collazuol. The sipm physics and technology—a review. *LAL Orsay*, 2012.
- [5] O. Daigle, P.-O. Quirion, and S. Lessard. The darkest EMCCD ever. In *High Energy, Optical, and Infrared Detectors for Astronomy IV*, volume 7742, pages 28–38. SPIE, 2010.
- [6] L. Gallego, J. Rosado, F. Blanco, and F. Arqueros. Modeling crosstalk in silicon photomultipliers. *Journal of Instrumentation*, 8(05):P05010, 2013.
- [7] A. Gola, A. Ferri, A. Tarolli, N. Zorzi, and C. Piemonte. SiPM optical crosstalk amplification due to scintillator crystal: effects on timing performance. *Physics in Medicine & Biology*, 59(13):3615, 2014.
- [8] H. Iams and B. Salzberg. The secondary emission phototube. *Proceedings of the Institute of Radio Engineers*, 23(1):55–64, 1935.
- [9] K. D. Irwin and G. C. Hilton. Transition-edge sensors. *Cryogenic particle detection*, pages 63–150, 2005.
- [10] A. Khandelwal, S. Jeram, R. Dungee, A. W. Lau, A. Lau, E. Sun, P. Van-Lane, S. Chen, A. Tohuvavohu, and T. S. Li. Beyond ccds: characterization of scmos detectors for optical astronomy. In *X-Ray, Optical, and Infrared Detectors for Astronomy XI*, volume 13103, pages 303–324. SPIE, 2024.
- [11] A. W. Lau, M. Shafiee, G. F. Smoot, B. Grossan, S. Li, and Z. Maksut. On-sky silicon photomultiplier detector performance measurements for millisecond to sub-microsecond optical source variability studies. *Journal of Astronomical Telescopes, Instruments, and Systems*, 6(4):046002–046002, 2020.
- [12] A. W. K. Lau, Y. Y. Chan, M. Shafiee, G. F. Smoot, and B. Grossan. Development of position-sensitive photon-counting imager for ultra-fast astronomy. In *X-Ray, Optical, and Infrared Detectors for Astronomy X*, volume 12191, pages 312–329. SPIE, 2022.
- [13] A. W. K. Lau, N. Shaimoldin, Z. Maksut, Y. Y. Chan, M. Shafiee, B. Grossan, and G. F. Smoot. Initial on-sky performance testing of the single-photon imager for nanosecond astrophysics (spina) system. *IEEE Transactions on Instrumentation and Measurement*, 2023.
- [14] A. Lehmann, A. Britting, W. Eyrich, C. Pizzolotto, A. Teufel, M. Düren, K. Föhl, M. Hoek, S. Lu, G. Schepers, et al. Performance studies of microchannel plate PMTs in high magnetic fields. *Nuclear Instruments and Methods in Physics Research Section A: Accelerators, Spectrometers, Detectors and Associated Equipment*, 595(1):173–176, 2008.
- [15] S. Li, G. F. Smoot, B. Grossan, A. W. K. Lau, M. Bekbalanova, M. Shafiee, and T. Stezelberger. Program objectives and specifications for the ultra-fast astronomy observatory. In *AOPC 2019: Space Optics, Telescopes, and Instrumentation*, volume 11341, pages 513–521. SPIE, 2019.

- [16] B. A. Mazin. Microwave kinetic inductance detectors. California Institute of Technology, 2005.
- [17] G. J. McLachlan and D. Peel. Finite mixture models. John Wiley & Sons, 2004.
- [18] F. Nagy, M. Mazzillo, L. Renna, G. Valvo, D. Sanfilippo, B. Carbone, A. Piana, G. Fallica, and J. Molnár. Afterpulse and delayed crosstalk analysis on a STMicroelectronics silicon photomultiplier. Nuclear Instruments and Methods in Physics Research Section A: Accelerators, Spectrometers, Detectors and Associated Equipment, 759:44–49, 2014.
- [19] G. Naletto, C. Barbieri, T. Occhipinti, I. Capraro, A. Di Paola, C. Facchinetti, E. Verroi, P. Zoccarato, G. Anzolin, M. Belluso, et al. Iqueye, a single photon-counting photometer applied to the ESO new technology telescope. Astronomy & Astrophysics, 508(1):531–539, 2009.
- [20] M. Shafiee, B. Grossan, G. Smoot, and A. W. K. Lau. Characterization of two-layer al/tin microwave kinetic inductance detectors. In X-Ray, Optical, and Infrared Detectors for Astronomy XI, page PC131030S. SPIE, 2024.
- [21] N. Teranishi. Required conditions for photon-counting image sensors. IEEE transactions on electron devices, 59(8):2199–2205, 2012.
- [22] J. Tiffenberg, M. Sofo-Haro, A. Drlica-Wagner, R. Essig, Y. Guardincerri, S. Holland, T. Volansky, and T.-T. Yu. Single-electron and single-photon sensitivity with a silicon Skipper CCD. Physical review letters, 119(13):131802, 2017.
- [23] S. Vinogradov. Analytical models of probability distribution and excess noise factor of solid state photomultiplier signals with crosstalk. Nuclear Instruments and Methods in Physics Research Section A: Accelerators, Spectrometers, Detectors and Associated Equipment, 695:247–251, 2012.

## A Remarks on the Detection Limit for detecting photon deficit

In the main text of this work, we exclusively focus on the use case, in which there is a ultra-fast astronomical transient that suddenly brightens up, thus delivering an unusual increment of photons counts over a very short time window.

As a complement, there is also another type of ultra-fast astronomical transients, that instead of a sudden brightening, a sudden dimming is observed. A more familiar astrophysical phenomenon of this type (on a longer time scale) is the observation of exoplanets transit. Hereafter, we would refer to this type of events as photon deficit.

The detection limit formulation for detecting photon deficit is simply:

$$Pr(N_{\text{det}} \leq N_{\text{thr},-} | \delta t, n_{\text{sky}}, n_{\text{dark}}, p_{\text{cross}}) \leq \text{FAR} \cdot \delta t, \quad (13)$$

and

$$Pr(A_{\text{det}} \leq A_{\text{thr},-} | \delta t, n_{\text{sky}}, n_{\text{dark}}, p_{\text{cross}}) \leq \text{FAR} \cdot \delta t. \quad (14)$$

However, these criteria are rarely used. As the bin time shortens, the expected number of photons per bin decreases significantly, and the detection threshold may fall below zero, leading to a non-physical detection limit. For example, with a background flux of  $1 \times 10^6$  counts per second and a bin size of 1 *ns*, it is likely that most bins will capture no photons at all, causing the detection threshold to drop to a nonphysical value.